Available online at www.sciencedirect.com

ScienceDirect

Procedia CIRP 118 (2023) 643–648

www.elsevier.com/locate/procedia

16th CIRP Conference on Intelligent Computation in Manufacturing Engineering, CIRP ICME '22, Italy

Porosity Examination of Additive Manufactured Parts and Effects of Infill Parameters

Osman Bodur[a,*], Eva M. Walcher[a], Alexandru Sterca[b], Clemens Sulz[a], Roxana-Anamaria Calin[b] Numan M. Durakbasa[a], Friedrich Bleicher[a]

[a] *TU Wien, Institute of Production Engineering and Photonic Technologies, Wien 1030, Austria*
[b] *Technical University of Cluj-Napoca, Faculty of Industrial Engineering, Robotics and Production Management, Cluj-Napoca, Romania*

* Corresponding author. Tel.: +43-676-576-0023 ; *E-mail address:* osman.bodur@tuwien.ac.at

Abstract

Additive manufacturing is gaining a significant place in Industry 4.0-driven environments, primarily due to the requirements for smoothly and quickly generatively designed components as opposed to multiple machining processes. The internal structure of the manufactured components has different geometric specifications depending on the filling density (80% to 100%) and filling pattern (lines, grid, triangles, etc.). This paper attempts to define the porosity of the additively manufactured parts depending on the infill parameters that affect the mechanical characterization of the parts using industrial computed tomography and observe the internal lattice structures and pattern-to-pore ratios of the manufactured parts.

Keywords: Additive manufacturing; Computer tomography; Porosity; Precision engineering

1. Introduction

Additive manufacturing is gaining increasing importance in fields such as rapid prototyping, medicine, aerospace and Industry 4.0 concepts due to its flexibility and rapid and direct CAD-to-Product capabilities. In particular, Fused deposition modeling has seen a rise in popularity due to the simplicity of the technology and the reduced cost of materials. However, all of these advantages are offset by the low surface quality and dimensional and geometric accuracy of the components obtained by using these technologies. Studies are being performed with good results on compensation methods [1] to mitigate these disadvantages by employing iterative correction loops. Research is also performed with good results in determining the effects of the main FDM process parameters on the quality of additive manufactured parts [2] and if predictive models for the ideal process parameters are feasible [3, 4]. The low quality of additive manufactured parts is especially challenging in the case of miniaturization of components [5], where studies [6] are performed employing high precision metrology and non-destructive measurement techniques for quality assessment and assurance of these components.

Nomenclature

CAD	Computer-Aided Design
CAM	Computer-Aided Manufacturing
FDM	Fused Deposition Modeling
STL	Standard Triangle Language – file format
PLA	Polylactic Acid

One of the most critical characteristics of additive manufactured parts is the infill pattern and density, which can affect the mechanical behavior [7, 8, 9, 10] and the dimensional, geometric, and surface quality of 3d printed components [11]. Infill pattern geometry and density also influence the total printing time of the component, as indicated by comparative studies [12], placing limits on choosing a compromise between part quality, mechanical behavior, and manufacturing productivity and cost. Complex bio-inspired infill patterns have

10.1016/j.procir.2023.06.110

also been studied [13, 14] to determine their capabilities from a mechanical behavior, economic, and sustainability standpoint.

In situations where the mass and density of the additive manufactured component are critical, infill pattern and percentage play an essential role. This study analyses the discrepancy between the expected mass, density, and infill percentage and the actual values of these characteristics and attempts to identify the root cause of the differences. To this end, a series of test parts are manufactured by FDM technology using eco-PLA material. The samples are fabricated with different infill patterns and percentages and subjected to Computed Tomography to determine the difference between the nominal and actual infill percentage as well as discrepancies in mass and density. The results are cross-correlated with the total manufacturing time and the time needed for printing the infill, informing decisions on the best choice of infill geometry for the desired application.

2. Theoretical and Experimental Parts

2.1. CAD Process

The geometry of the test samples is chosen and created as per standard ISO 10791-7 [15] to ensure consistent results across studies. The cad model is displayed in Fig. 1. with all relevant dimensional and geometric characteristics as specified in ISO:1101, which governs geometric product specifications. [16]

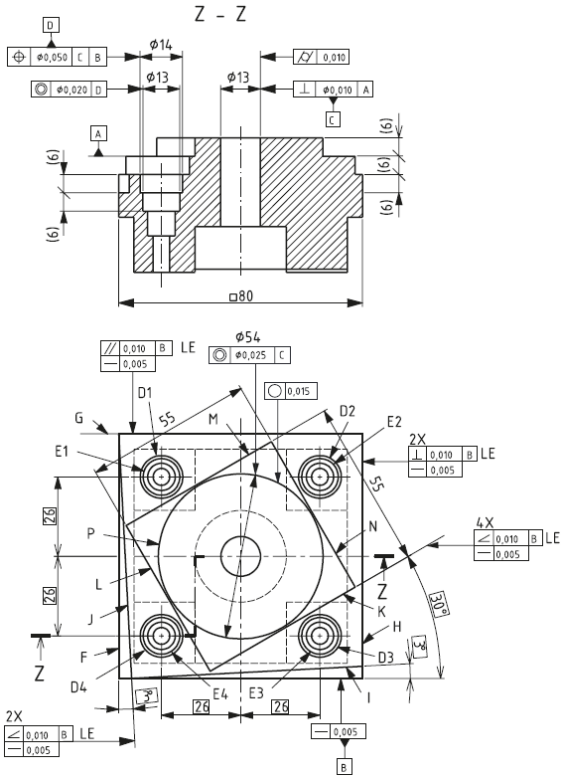

Fig. 1. Positioning and contouring workpiece in ISO 10791-7, 80x80 mm.

2.2. CAM Process

The CAM design process is performed using the Ultimaker Cura [17] slicing software. G-code manufacturing program is realized with 80% and 90% infill percentages in different infill pattern geometries. A preview of the examined patterns and the G-code generated for manufacturing are presented in Fig 2.

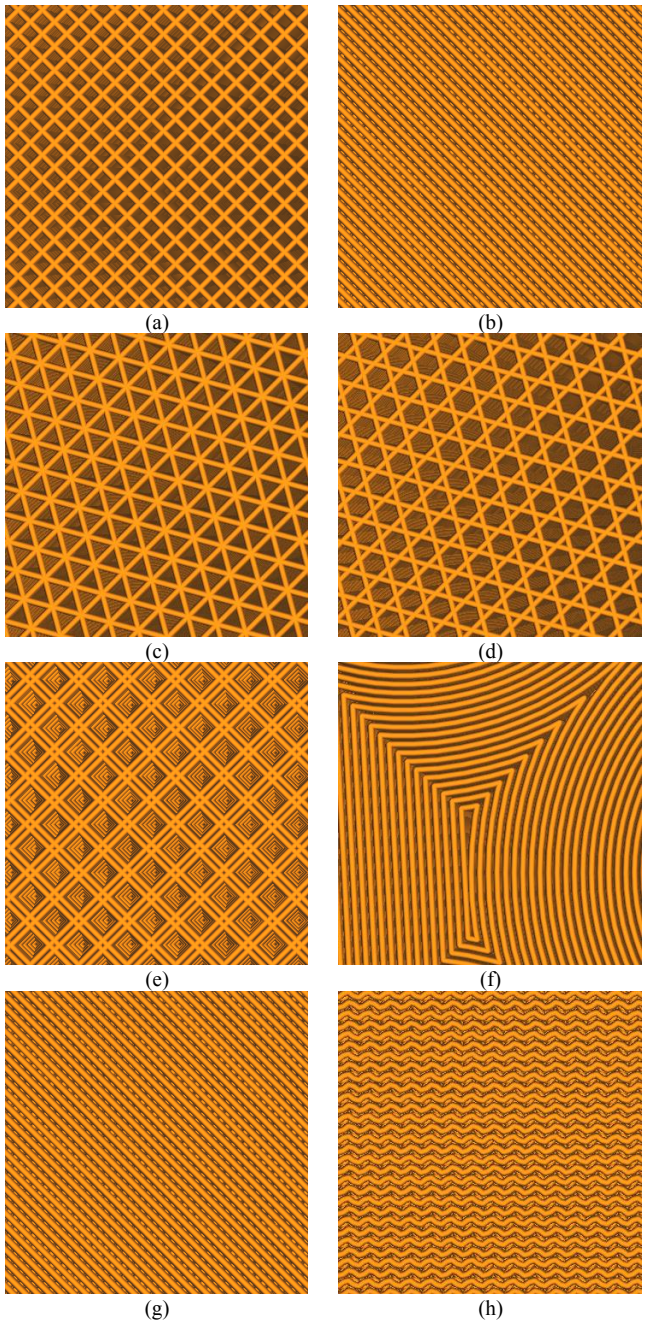

Fig. 2. Infill pattern geometries (a) Grid; (b) Lines; (c) Triangles; (d) Trihexagon; (e) Octet; (f) Concentric; (g) Zigzag; (h) Gyroid.

2.2.1. FDM - Additive Manufacturing

After creating and designing the CAD model (Fig. 3a.) of sample geometry, the data is converted to the STL file format (Fig. 3b.) in order to generate G-code (Fig. 3c.) through Ultimaker Cura software. The Additive Manufacturing CAM process is realized using the Octo Print User Interface, a platform to manage the 3D printer via the network connection. A flow chart is presented in Fig. 3. A manufactured component from 18 workpieces is available in Fig. 3d.

Eighteen test samples are manufactured from eco-PLA [18] filament on an Anycubic Mega X 3D Printer [19] using different infill patterns as demonstrated in Fig. 4a. The test samples are manufactured with the same main process parameters to ensure consistency of the results. The manufacturing parameters are, Nozzle temperature 200ºC, heated bed temperature 60ºC, speed 60 mm/s, cooling 75%, and layer height 0.2mm. The manufacturing is done by a 0.4 mm nozzle and 1.75 mm diameter filament.

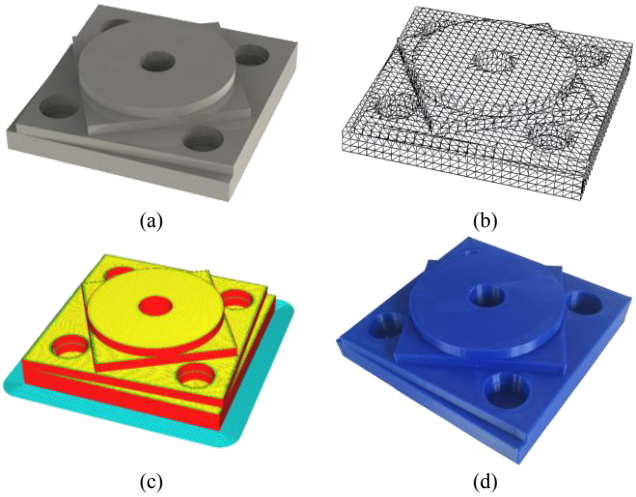

(a) (b) (c) (d)

Fig. 3. (a) CAD Model; (b) STL Model; (c) G-Code Model (d) Additive Manufactured Model.

Two samples are manufactured with 80% and 90% infill density for each infill pattern employed. Two samples with 100% infill are also manufactured to provide a control point. The infill type and percentage are presented in Table 1.

Table 1. Infill pattern type and percentages of additive manufactured models.

Part numbers	Infill pattern type	Infill percentages (%)
1 – 2	Grid	80 and 90
3 – 4	Lines	80 and 90
5 – 6	Triangles	80 and 90
7 – 8	Trihexagon	80 and 90
9 – 10	Octet	80 and 90
11 – 12	Concentric	80 and 90
13 – 14	Zigzag	80 and 90
15 – 16	Gyroid	80 and 90
17 – 18	Filled Up	100

2.3. Measurement Process

Computer tomography is performed on the test samples employing a Zeiss Metrotrom [20] tomograph in Fig. 4c. The parameters used for scanning are 120kV at 230 µA and 500 ms integration time. Five images are integrated for each slice to increase the signal-to-noise ratio. The sample is scanned at a distance of 425 mm from the sensor, giving a voxel size of 0.113mm. The point cloud for 3D reconstruction is interpolated from 1050 slices representing a full 360deg scan at a step angle of 0.34deg. Data analysis is performed using the GOM volume inspect software [21].

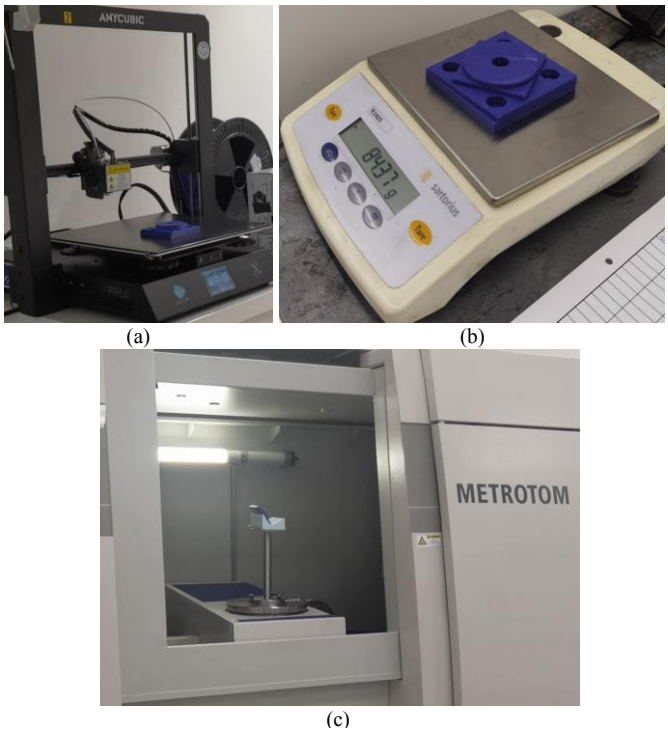

(a) (b) (c)

Fig. 4. (a) Anycubic Mega X 3D Printer; (b) Precision Scale; (c) Computed Tomography Metrotom..

The mass of the parts is measured using a Sartorius TE3102S [22] precision scale as illustrated in Fig. 4b. These measurements are used to determine the actual density of the samples for each infill pattern and percentage.

3. Results

The results of all measurements in the form of actual volume, part volume without defects, and volume defects in cm^3 depending on the infill pattern type and infill percentage are detailed by the advanced evaluation software as indicated in Table 2. It is possible to infer that the total volumes of the outer hull values are in close proximity to each other. Nevertheless, the highest value of the volume of the outer hull occurs at the octet infill pattern with 80% and the highest porosity is observed at the trihexagon with the 80% infill percentage.

Table 2. Volume, volume defects and porosity of additive manufactured parts.

Infill pattern	Infill Percentage (%)	Total Volume of outer hull (cm^3)	Part volume without defects (cm^3)	Total volume defects (cm^3)	Porosity (%)
Grid	80.00	89.522	70.939	18.583	20.758
Grid	90.00	89.340	75.496	13.845	15.497
Lines	80.00	89.213	80.456	8.757	9.816
Lines	90.00	89.216	85.262	3.954	4.432
Triangles	80.00	89.541	70.899	18.642	20.819
Triangles	90.00	89.685	76.478	13.207	14.726
Trihexagon	80.00	89.524	67.921	21.603	24.131

Trihexagon	90.00	89.618	74.461	15.157	16.913
Octet	80.00	89.504	72.245	17.259	19.283
Octet	90.00	89.579	76.782	12.797	14.286
Concentric	80.00	76.237	73.474	2.762	3.623
Concentric	90.00	88.707	86.523	2.041	2.300
Zigzag	80.00	82.467	80.560	1.907	2.313
Zigzag	90.00	88.878	87.599	1.279	1.439
Gyroid	80.00	87.301	79.184	8.117	9.298
Gyroid	90.00	89.013	88.499	0.514	0.577
Filled Up	100.00	88.244	88.043	0.201	0.227
Filled Up	100.00	88.220	88.096	0.125	0.141

The internal gaps resulting from the infill pattern are presented in Fig. 5., in the form of volume defects, color-coded by the volume of each individual gap.

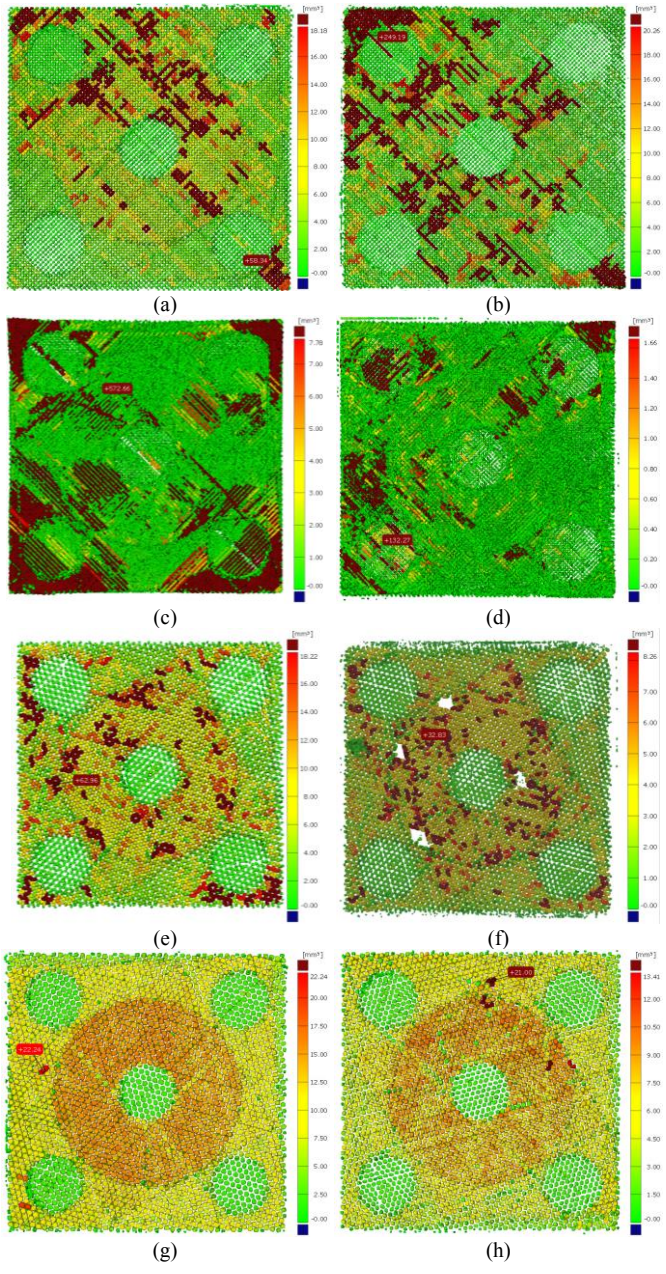

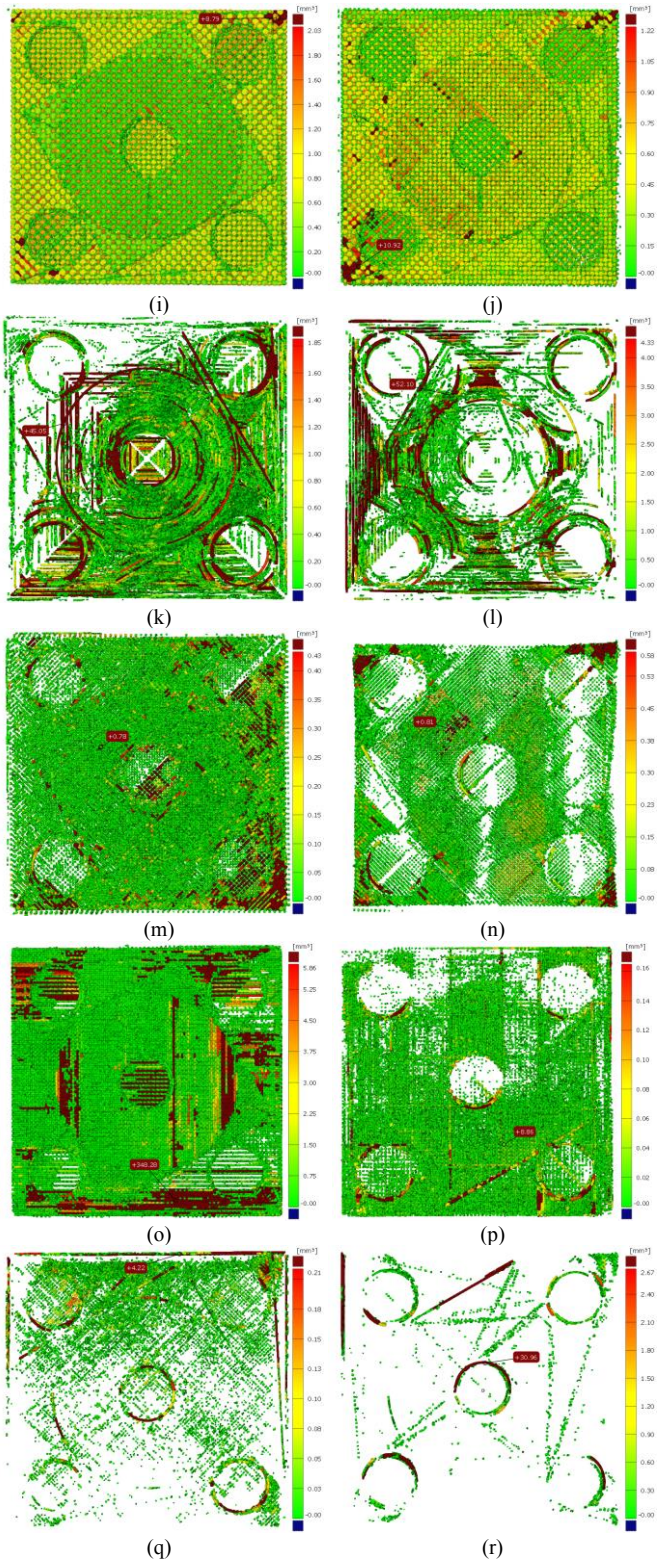

Fig. 5. Volume defect maps of additive manufactured models (a) Grid 80%; (b) Grid 90%; (c) Lines 80%; (d) Lines 90%; (e) Triangles 80%; (f) Triangles 90%; (g)Trihexagon 80%; (h) Trihexagon 90%; (i) Octet 80%; (j) Octet 90%; (k) Concentric 80%; (l) Concentric 90%; (m) Zigzag 80% (n) Zigzag 90%; (o) Gyroid 80%; (p) Gyroid 90%; (q) Full-1 100% (r) Full-2 100% .

Volume defect maps of additive manufactured models are represented in Fig. 5. The defects maps are useful to see the mean defects values as the colored legends; one of them is the dark brown color shows outliers from the average range of volume defects. The green colors highlight the volume defects

in minimum scales. Grid, triangles, and trihexagon infill patterns with 80% and 90% infill, illustrated in Fig. 5a., 5b., 5e., 5f., 5g. and 5h., have regular porosity distribution. The Infill pattern lines with 80% infill has irregularities at the corners of test samples, especially in those areas where volume defects are higher than the lines with 90% infill, as seen in Fig. 5c. and 5d. When infill percentages are increased from 80% to 90%, the average sizes of the volume defects are decreased for the infill patterns lines, triangles, trihexagon, octet, and gyroid. For instance, the average volume defect sizes of lines infill patterns are reduced from max 7.78 mm^3 to max 1.66 mm^3 in the legend of the volume defect maps seen in Fig. 5c. and 5d. On the other side, the average volume defect sizes of the grid, concentric and zigzag infill patterns are enlarged, as seen in Fig. 5. even though the total volume defects of those infill patterns are diminished seen in Table 2. The distribution of the volume defect size according to the infill pattern types is the smallest with the 0.16 mm^3 value on the gyroid infill pattern with 90% infill, as illustrated in the legend on the graph Fig. 5p. Besides, the lines infill pattern has the largest volume defect size, which is 572.66 mm^3, although the total volume defects of that infill pattern are not maximal, according to Table 2.

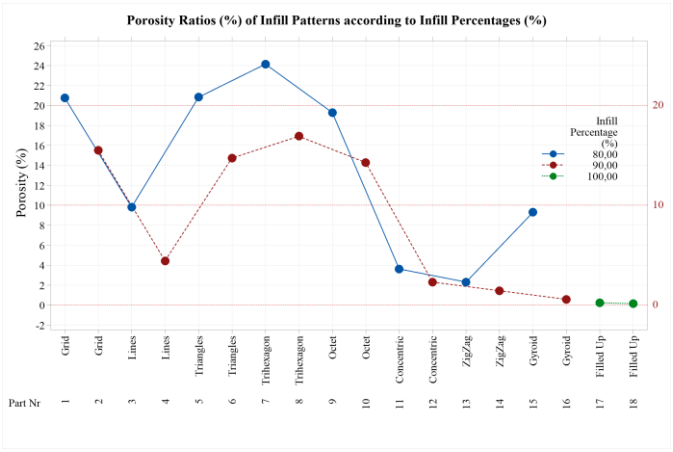

(a)

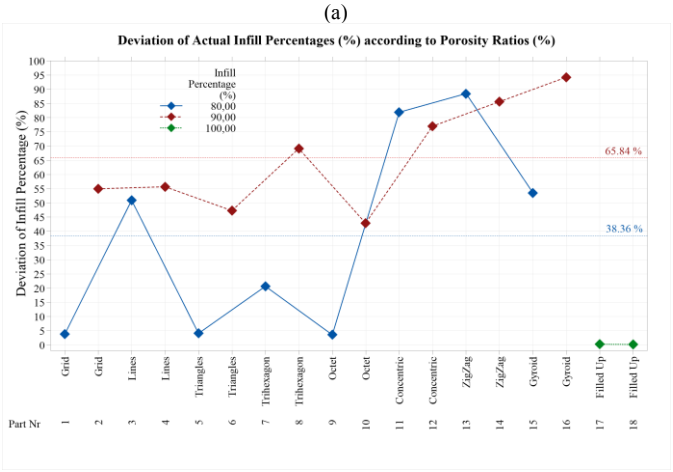

(b)

Fig. 6. Porosity ratios (%) of infill patterns according to the infill percentages.

From an analysis of the 3D structure of the resulting infill pattern, it is evident that as the complexity of the infill geometry increases, the quality of the printed pattern decreases, as is visible, especially in the case of zigzag, gyroid, and concentric. The effects of over and under extrusion are also evident, as well as material overflow due to pressure build-up inside the nozzle.

An analysis of expected versus actual infill percentage with the reference lines 0%, 10%, and 20% is shown in Fig. 6a. The most proximate porosity ratios of infill patterns to the reference lines are detected at the grid, triangles, octet, and filled up infill patterns, as shown in Fig. 6a, whose values are respectively 3.79%, 4.10%, 3.59%, and 0.18% (average value for filled up) as observed in Fig. 6b. The measurement results compare to infill percentages; while the infill percentage is 80%, the workpiece with a grid infill pattern has only a 3.79% deviation from solid geometries, but when the infill percentage is 90%, that value is abruptly increased by 54.97%. The triangles infill pattern with an 80% infill percentage has the slightest deviation between expected and actual infill percentage. The minor deviation for the 90% infill percentage is seen in the octet infill pattern and the deviation for the 100% infill percentage is predictably minimal as observed in Fig. 6b.

The statistical results indicate that the geometric complexity of the infill pattern has a high impact on the actual infill percentage of the manufactured part. Complex infill pattern geometries like concentric, zigzag, and gyroid have higher deviation between expected infill and actual infill percentages.

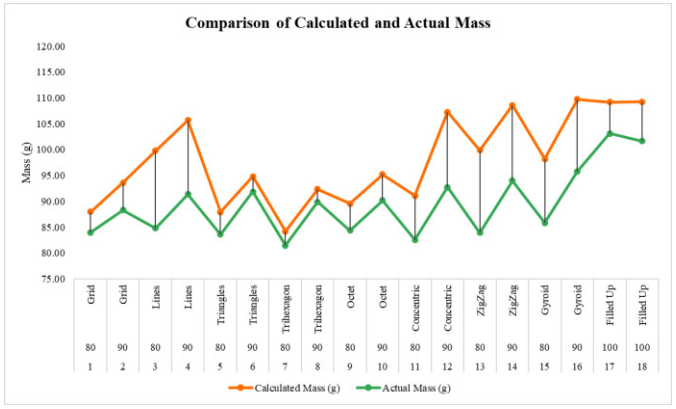

Fig. 7. Comparison of calculated and actual mass values.

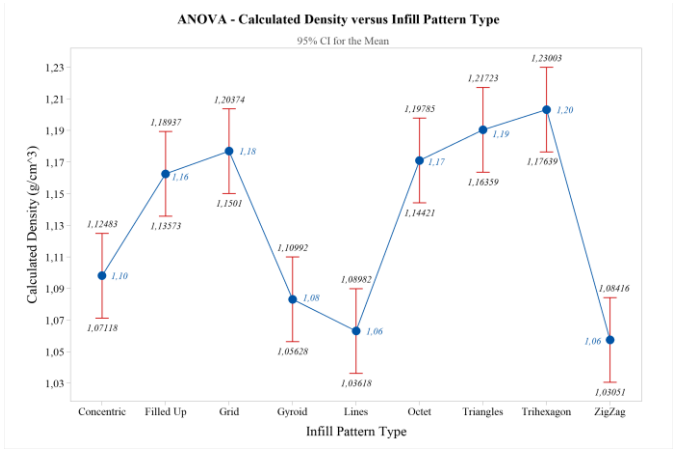

Fig. 8. ANOVA statistical analysis for calculated density versus infill pattern.

The calculated and actual mass comparison is evaluated in Fig. 7. According to the actual mass, the density of the infill pattern geometries is calculated and determined the mean

values with 95% confidence intervals with ANOVA statistical analysis, as delineated in Fig. 8. The 90 % gyroid infill pattern has the heaviest calculated mass in Fig. 7. due to its part volume without defects. The trihexagon infill pattern with 80% has the lowest mass value of 84.22 g and has the closest density value as 1,20 g/cm^3 to the eco-PLA density (1,25 g/cm^3) in Fig. 8.

These results indicate that geometries that require a high rate of fast changes in the direction of the printing nozzle, as well as a high number of filament retraction operations, will lead to lower quality infill patterns and thus a high discrepancy between expected and actual part infill percentage, mass and density. Errors in manufactured infill patterns can lead to density variations, and changes in the mechanical properties of the additive manufactured parts. In cases where these characteristics are critical, the choice of infill pattern is critical. However, if the application requires a specific infill geometry, the parameters of the machine used to manufacture the parts must be fine-tuned. The parameters which affect infill quality and accuracy are flow rate, material retraction, acceleration, speed, and backlash compensation.

4. Conclusions and Discussion

The study focuses on the effect of infill pattern geometry and percentage on the actual infill percentage, mass, and density of the additive manufactured parts.

A strong correlation between the complexity of the infill pattern geometry and the actual infill parameters and quality is observed in the results, indicating that for applications where the infill percentage, mass and density of the manufactured parts are critical, special care must be taken in fine-tuning the process parameters in the form of flow rate, printing speed and acceleration, filament retraction distance and speed.

A compromise between infill geometry characteristics desired part mechanical properties, and printing time also exists, thus the infill geometry must be chosen in order to satisfy mechanical and functional specifications of the manufactured component but with an emphasis on economic and time constraints. Future studies can be performed on developing mathematical predictive models for the ideal process parameters according to infill geometry complexity which allows for the lowest discrepancy between expected and actual values of manufactured components' mass, density, and infill percentage.

References

[1] Bodur, Osman; Stepanek, Vojtech; Walcher, Eva Maria & Durakbasa, Numan (2020). Precision in Additive Manufacturing, Optimization and Evaluation of the Accuracy of 3D Printer based on GPS System, Proceedings of the 31st DAAAM International Symposium, pp.0963-0972, B. Katalinic (Ed.), Published by DAAAM International, ISBN 978-3-902734-29-7, ISSN 1726-9679, Vienna, AustriaDOI: 10.2507/31st.daaam.proceedings.134

[2] Sterca, A.D. et al. (2022). Evaluation of Fused Deposition Modeling Process Parameters Influence on 3D Printed Components by High Precision Metrology. In: Durakbasa, N.M., Gençyılmaz, M.G. (eds) Digitizing Production Systems. Lecture Notes in Mechanical Engineering. Springer, Cham. https://doi.org/10.1007/978-3-030-90421-0_24

[3] Grozav, S.D.; Sterca, A.D.; Kočiško, M.; Pollák, M.; Ceclan, V. Feasibility of Predictive Models for the Quality of Additive Manufactured Components Based on Artificial Neural Networks. Machines 2022, 10, 128. https://doi.org/10.3390/machines10020128

[4] Khanzadeh, M., Rao, P., Jafari-Marandi, R., Smith, B. K., Tschopp, M. A., and Bian, L. (December 21, 2017). "Quantifying Geometric Accuracy With Unsupervised Machine Learning: Using Self-Organizing Map on Fused Filament Fabrication Additive Manufacturing Parts." ASME. J. Manuf. Sci. Eng. March 2018; 140(3): 031011. https://doi.org/10.1115/1.4038598

[5] Durakbasa, N.M., Bauer, J.M., Bodur, O., Poszvek, G. (2019). Challenges of Miniaturizing a Precision Gear. In: Durakbasa, N., Gencyilmaz, M. (eds) Proceedings of the International Symposium for Production Research 2018. ISPR 2018. Springer, Cham. https://doi.org/10.1007/978-3-319-92267-6_21

[6] Durakbasa, N.M. et al. (2019). Additive Miniaturized-Manufactured Gear Parts Validated by Various Measuring Methods. In: Majstorovic, V., Durakbasa, N. (eds) Proceedings of the 12th International Conference on Measurement and Quality Control - Cyber Physical Issue. IMEKOTC14 2019. Lecture Notes in Mechanical Engineering. Springer, Cham. https://doi.org/10.1007/978-3-030-18177-2_25

[7] Lubombo, Christian & Huneault, Michel. (2018). Effect of Infill Patterns on the Mechanical Performance of Lightweight 3D-Printed Cellular PLA Parts. Materials Today Communications. 17. 10.1016/j.mtcomm.2018.09.017.

[8] Derise, Mohammad & Zulkharnain, Azham. (2021). Effect of Infill Pattern and Density on Tensile Properties of 3D Printed Polylactic acid Parts via Fused Deposition Modeling (FDM). International Journal of Mechanical & Mechatronics Engineering. 20. 54-62.

[9] Pandzic, A[di]; Hodzic, D[amir] & Milovanovic, A[leksa] (2019). Effect of Infill Type and Density on Tensile Properties of PLA Material for FDM Process, Proceedings of the 30th DAAAM International Symposium, pp.0545-0554, B. Katalinic (Ed.), Published by DAAAM International, ISBN 978-3-902734- 22-8, ISSN 1726-9679, Vienna, Austria DOI: 10.2507/30th.daaam.proceedings.074

[10] Dave, H. K., Patadiya, N. H., Prajapati, A. R., & Rajpurohit, S. R. (2021). Effect of infill pattern and infill density at varying part orientation on tensile properties of fused deposition modeling-printed poly-lactic acid part. Proceedings of the Institution of Mechanical Engineers, Part C: Journal of Mechanical Engineering Science, 235(10), 1811–1827. https://doi.org/10.1177/0954406219856383

[11] Lalegani Dezaki, M.; Ariffin, MKAM; Serjouei, A.; Zolfagharian, A.; Hatami, S.; Bodaghi, M. Influence of Infill Patterns Generated by CAD and FDM 3D Printer on Surface Roughness and Tensile Strength Properties. Appl. Sci. 2021, 11, 7272. https://doi.org/ 10.3390/app11167272

[12] Yazar, Alparslan & Top, Neslihan & Bülbül, Ramazan & şahin, Ismail. (2021). Effect of Infill Density and Infill Pattern on Mechanical Properties in Fused Deposition Modeling (FDM).

[13] Dev, S., Srivastava, R. Effect of infill parameters on material sustainability and mechanical properties in fused deposition modelling process: a case study. Prog Addit Manuf 6, 631–642 (2021). https://doi.org/10.1007/s40964-021-00184-4

[14] Podroužek, J.; Marcon, M.; Ninčević, K.; Wan-Wendner, R. Bio-Inspired 3D Infill Patterns for Additive Manufacturing and Structural Applications. Materials 2019, 12, 499. https://doi.org/10.3390/ma12030499

[15] ISO 10791-7:2020; Test conditions for machining centres — Part 7: Accuracy of finished test pieces

[16] ISO 1101; Geometrical product specifications (GPS) - Geometrical tolerancing - Tolerances of form, orientation, location, and run-out; 2020.

[17] Ultimaker Cura Software. Available online: https://ultimaker.com/software/ultimaker-cura (accessed: 31.05.2022)

[18] Technical Data Sheet. 3D Jake, Austria. Available online: https://c-3d.niceshops.com/upload/file/Technical_Data_Sheet[0].pdf (accessed 31.05.2022)

[19] Anycubic Mega X. Anycubic, China. Available online: https://de.anycubic.com/products/mega-x (accessed: 31.05.2022)

[20] METROTOM Technische Daten. Carl Zeiss Industrielle Messtechnik GmbH, Germany; 2013.

[21] GOM volume inspect. Zeiss Gom Metrology. Available online: https://www.gom.com/en/products/gom-suite/gom-volume-inspect-pro (accessed: 31.05.2022)

[22] Sartorius Talent Sartorius Gem Gold. Sartorius AG, Göttingen; 2004. Publication No.: WTE6001-d04052.